ELSEVIER

Thermochimica Acta 287 (1996) 261–278

thermochimica acta

The effects of heat and mass transfer in thermogravimetrical analysis. A case study towards the catalytic oxidation of soot

John P.A. Neeft, Fred Hoornaert, Michiel Makkee, Jacob A. Moulijn*

Industrial Catalysis, Department of Chemical Engineering, Delft University of Technology, Julianalaan 136, 2628 BL Delft, The Netherlands

Received 27 February 1996; accepted 26 March 1996

Abstract

A convenient model has been developed which qualitatively describes the heat and oxygen mass transport within a TGA sample crucible. The major conclusion from this model and from experimental observations was that for exothermal reactions, heat- and mass-transfer limitations can significantly influence the results of thermogravimetrical analysis. Therefore, it is crucial to use small, diluted samples, in particular for quantitative thermo-analytical measurements. It is recommended that the occurrence of heat- and mass-transport limitations be assessed by variation of the sample mass by at least a factor of ten.

The model provides an explanation for the double-peak-shaped curves which are often observed when studying the catalysed oxidation of a model soot. The first peak is attributed to a thermal runaway reaction, which occurs when the sample is relatively large and when it is not diluted with silicon carbide. It is shown that the occurrence of the two peaks is caused by a combination of heat- and mass-transport limitations within the TGA sample.

Keywords: Heat-transport limitations; Mass-transport limitations; Model; Oxidation; Soot

1. Introduction

Thermo-analytical techniques are commonly used in research laboratories. Examples of such techniques are thermogravimetrical analysis (TGA), differential

* Corresponding author. Tel., +31 15 2785008; fax, +31 15 2784452.

PII S0040-6031(96)03002-X

thermal analysis (DTA) and differential scanning calorimetry (DSC). Thermo-analytical (TA) techniques have certain advantages and disadvantages in comparison with the more traditional flow-reactor techniques which are also widely employed. An important advantage of TA techniques is their convenience, as small sample sizes can be used and the analyses are usually rather fast compared with flow-reactor experiments. The main disadvantage of TA techniques is that the sample is enclosed in a small crucible. As a result, the gas feed flows around the sample, instead of through the sample as is the case in most flow-reactor samples. The sample is more or less isolated from its surroundings. Therefore, heat- and mass-transfer limitations between the sample and the surroundings can easily occur when the chemical or physical processes in the sample are fast. In conventional packed bed reactors, such limitations can also occur but only within or around the individual sample particles. As a consequence, the characteristic diameter of the volume in which these limitations occur differs considerably: this diameter is in the mm range in TA samples whereas it is in the (sub-)μm range in flow-reactor samples. Of course, in flow-reactors gradients can also be important when the dimensions of the reactor are considered instead of those of a particle. These gradients are dealt with in the literature where criteria are given enabling avoidance of these gradients [1].

Many examples of such heat- and mass-transfer limitations in TA techniques can be found in the literature. Mass-transfer limitations have, for example, been reported in the potassium-carbonate-catalysed carbon steam gasification [2], in the oxidation of porous carbonaceous materials [3,4], and in many other oxidation reactions. When the chemical or physical process under study is exothermal, then heat-transfer limitations can lead to runaway reactions. Such runaway reactions have, for instance, been reported for coal oxidation carried out in TGA [5].

To our knowledge, a systematical study of the effect of both heat and mass transfer on the results of TA experiments has never been carried out. Knowledge of the combined heat- and mass-transfer limitations would enable a better estimation of the validity of results obtained with TA techniques.

The aim of this study is to substantiate some of the above conclusions by a numerical simulation towards heat and mass transport in thermal analysis. As an example, the catalytic oxidation of soot in combined TGA/DSC is studied. The numerical model is used to indicate qualitatively the importance of heat- and mass-transfer limitations, as well as to give an explanation for the unusual TGA/DSC curves observed for the catalytic oxidation of soot.

The computer model is based on a model of Melling and coworkers [6], who used their model to study the influence of a number of experimental parameters on results obtained with DTA. Our model has a different goal. By a proper description of the heat- and oxygen mass-transfer, local temperatures and oxygen concentrations in the sample are calculated, which enable the calculation of overall TGA profiles. These numerical results are compared with experimental TGA profiles. TGA is a technique that resembles DTA in the sense that sample geometry and the directions of heat and mass transfer are similar.

2. Experimental

2.1. Soot

As was explained in more detail elsewhere (Chapter 2 of Ref. [7]), we chose to work with a flame soot (namely, Printex-U) which was supplied by Degussa AG.

2.2. Catalyst materials

Fe_2O_3 was prepared by calcination of $Fe(NO_3)_3 \cdot 9H_2O$ at 875 K for two hours. Co_3O_4 was prepared by calcination of $Co(NO_3)_2 \cdot 6H_2O$ at 675 K for two hours. It is demonstrated elsewhere (Chapter 3 of Ref. [7]) that the soot oxidation activity of Co_3O_4 largely depends on the calcination temperature, i.e. at high calcination temperature (> 675 K) cobalt oxide is less active than cobalt oxide obtained by calcination at 675 K. The catalysts were milled and sieved before use; catalyst particles with diameters smaller than 125 μm were used.

2.3. Mixtures of soot and catalyst

Mixtures of soot and catalyst were milled using a mechanical agate mill (Fritsch, pulverisete type 05.202: cup diameter 45 mm, cup height 37 mm, 4 agate mill balls of 10 mm diameter). A catalyst-to-soot ratio of two on a weight basis was used.

2.4. Thermogravimetrical analysis (TGA)

TGA was performed on an STA 1500H thermobalance of Polymer Laboratories. This thermobalance allowed simultaneous measurement of TGA and DSC profiles. The DSC profile was measured by two thermocouples, one under the sample cup and one under a reference sample cup. A heating rate of 10 K min^{-1} was used. Oxidation experiments were performed in 50 Nml min^{-1} of 21 vol% O_2 in N_2; for experiments in an inert atmosphere 50 Nml min^{-1} of He was used.

3. Computer model

3.1. Model description

A schematic representation of the sample crucible and sample is given in Fig. 1. The crucible (or cup) and sample are divided into concentric rings. As the sample is in the form of a cylinder, temperature gradients can be divided into an axial and a radial contribution. Therefore, a two-dimensional heat transport model is needed to model the heat transport which results from these temperature gradients. As such a model would require rather large calculation times, a one-dimensional heat transport model was chosen, i.e. only heat transport in the radial direction was considered. This approximation has been shown to be valid at locations far from the extremes of the

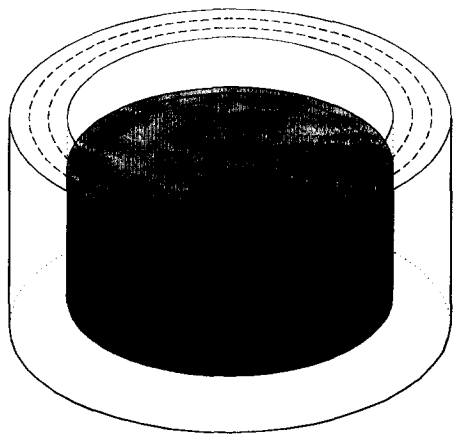

Fig. 1. Schematic representation of sample (dark) and cup (light).

cylinder and if the length-over-diameter ratio of the sample cylinder is larger than three [6].

The model is based on a heat and mass balance over these segments (concentric rings) within the sample. A detailed derivation of the model is given elsewhere (Chapter 4 of Ref. [7]). The model calculates temperatures, oxygen concentrations and reaction rates (which depend on temperature and oxygen concentration) in the segments as a function of time or TGA oven temperature, which is a linear function of time as a constant heating rate is chosen.

The description of the heat transport is based on Fourier's law, extended with a heat production term $\delta q_{\text{reaction}}/\delta t$ which accounts for the produced heat of reaction per unit of time

$$\rho C_p V \frac{\partial T}{\partial t} = k\nabla^2 T + \frac{\partial q_{\text{reaction}}}{\partial t} \tag{1}$$

in which ρ is density, C_p is heat capacity, V is volume, T is temperature, t is time, k is a constant and q is heat. This heat balance is evaluated in the radial direction of the segments of the sample and the sample cup.

Oxygen transport takes place from the gas bulk to the sample, i.e. in a vertical direction. As a first approximation, the oxygen concentration in the sample is considered to be homogeneous, i.e. oxygen diffusion in the sample is faster than the reaction rate. Under runaway conditions, where reaction rates become very high in comparison with the rate of oxygen supply, this might be a poor approximation.

The oxygen mass-transfer is described by the film model

$$J_{O_2} = k_{O_2} \frac{[O_2]_{\text{bulk}} - [O_2]_{\text{sample}}}{[O_2]_{\text{bulk}}} \tag{2}$$

in which J_{O_2} is the flux of oxygen to the sample, k_{O2} is an oxygen mass-transfer coefficient, $[O_2]_{bulk}$ is the oxygen concentration in the TGA feed gas, and $[O_2]_{sample}$ is the sample oxygen concentration. It is noted that only mass-transfer limitations from the gas bulk to the sample are considered; mass-transport limitations within the sample, e.g. due to pore diffusion limitations, are not taken into account.

Peculiar TGA/DSC profiles (examples of which are shown later in this paper) have been observed for the oxidation of soot in the presence of several catalysts. In this model study, Fe_2O_3 is taken as a representative catalyst. A number of reactions can take place when soot is oxidized catalytically by Fe_2O_3. Catalytic oxidation of carbon (soot) to carbon dioxide is the main reaction, in which Fe_2O_3, or more specifically surface Fe_2O_3, acts as a catalyst. It is believed that at higher temperatures, the reduction of bulk Fe_2O_3 by carbon can also take place. This reaction was observed by TGA with an Fe_2O_3/Printex-U sample in an inert (He) gas flow. Re-oxidation of Fe_3O_4 is a final reaction that should be taken into account. Thus, the three reactions considered in the model are

$$C + O_2 \xrightarrow{Fe_2O_3,\,surface} CO_2 \tag{3}$$

$$6Fe_2O_{3,bulk} + C \longrightarrow 4Fe_3O_{4,bulk} + CO_2 \tag{4}$$

$$4Fe_3O_{4,bulk} + O_2 \longrightarrow 6Fe_2O_{3,bulk} \tag{5}$$

3.2. Parameters and procedures

Physical constants were obtained from the literature, if possible. Densities were assumed to be independent of temperature; all other constants were calculated at 773 K. The sample density was measured (TGA sample cup volume and the weight of the sample fitting in this cup). The value obtained (598.4 kg m^{-3}) is on the high side of the density range as calculated from the densities of Fe_2O_3 and soot (60–1040 kg m^{-3}). This is probably caused by an increase in the density of the soot when soot and Fe_2O_3 are mechanically milled in the sample preparation. The heat conductivity for Fe_2O_3 is not known; a value of 1 W m^{-1} K^{-1} is assumed, which is a typical value for pressed powder metal oxides [8]. The heat conductivity of amorphous carbon is about 2.35 W m^{-1} K^{-1} at 773 K [9], and the heat conductivity of the carbon/Fe_2O_3 sample (λ_{sample}) based on these two heat conductivities is 1.237 W m^{-1} K^{-1}. In the calculations, λ_{sample} has been varied between 1.237 and 0.155 W m^{-1} K^{-1} because the value of 1.237 W m^{-1} K^{-1} is also thought to be an upper limit, as the density of amorphous carbon is much higher than the density of soot. A full list of the parameters used in the numerical simulations is given elsewhere (Chapter 4 of Ref. [7]).

Heats of reaction were calculated from the heats of formation and heat capacities of carbon (graphite), oxygen, carbon dioxide, Fe_2O_3, and Fe_3O_4 [10,11]. Values are listed in Table 1.

Kinetic parameters for these three reactions were obtained from TGA experiments. Pre-exponential factors of reactions (3) and (4) were determined from a fit to the

Table 1
Kinetic parameters from the literature (E_a) and obtained from experimental data (k_0)

Reaction	Heat of reaction at 773 K/J(mol C)$^{-1}$ or J(mol Fe_2O_3)$^{-1}$	Activation energy E_a/kJ mol^{-1}	Pre-exponential factor k_0/s^{-1}
(3)	-3.939×10^5	201 [12]	5.625×10^{11}
(4)	2.264×10^4	300 [13, 14]	5.75×10^{15}
(5)	-8.829×10^4		

experimental data. A simple model was used in which temperature effects and oxygen depletion were not taken into account. Activation energies were taken from the literature: 200.8 kJ mol^{-1} for reaction (3) [12], and 300 kJ mol^{-1} for reaction (4) [13, 14]. The latter value was taken from data measured at temperatures much higher than the temperatures in this study. In the open literature, no activation energies were found for the appropriate temperature range. The pre-exponential factors were determined using: (*i*) these activation energies; (*ii*) TGA profiles of Fe_2O_3soot combustion using a very small sample (1 mg Printex-U which was diluted to avoid heating of the sample); and (*iii*) TGA profiles of carbothermic reduction of Fe_2O_3 to Fe_3O_4. Values of these pre-exponential factors are also listed in Table 1. The pre-exponential factor of reaction (5) was chosen to be infinitely high, as re-oxidation of Fe_3O_4 to Fe_2O_3 takes place at much lower temperatures than the other two reactions that are considered. In the temperature range under consideration, the rate of reaction (5) is determined by the availability of oxygen. A more detailed description of the determination of these values is given in Chapter 4 of Ref. [7].

3.3. Numerical simulations

Numerical simulations were performed on MSDOS-type 386 and 486 computers, the computer code was written in PASCAL. The sample was divided into 20 shells, the cup material into 3. A stability criterion as mentioned by Melling and coworkers [6]

$$\frac{(\Delta r)^2}{\frac{\lambda}{\rho C_p}\Delta t} \geqslant 3 \tag{6}$$

(in which Δr is the thickness of the shell, λ heat conductivity, ρ density, and C_p heat capacity) is fulfilled for both the sample and the cup if the integration step size Δt is smaller than 2.7×10^{-4} s. Therefore, a standard integration step size Δt of 1×10^{-4} s was employed. At this step size, results were found to be independent of integration step size.

4. Results

4.1. Influence of sample mass on TGA curves

In early experiments it was observed that the TA curves of Printex-U oxidation, in tight contact with a number of catalysts, consisted of two peaks in both DSC and DTG (DTG is the time derivative of TGA). The first peak was always very steep and sharp whereas the second peak was broad and smooth. An example for a Co_3O_4 catalyst is shown in Fig. 2 for a sample size of about 3.5 mg Printex-U. The TGA curve is plotted against sample temperature in Fig. 2a, and the TGA and DSC curves are plotted against time in Fig. 2b. In Fig. 2b, the sample temperature is also plotted, as measured under the sample cup. Clearly, the temperature increased significantly in the first peak. This increased sample temperature is the cause of the non-singularity of the TGA curve in Fig. 2a.

Using an Fe_2O_3 catalyst, a similar TGA curve with two peaks was measured, which is shown as curve A in Fig. 3. In a subsequent experiment, the TGA run was interrupted after the first, sharp peak (curve B1 in Fig. 3). Restarting the experiment from a low temperature (curve B2) yielded only the smooth combustion peak, the first, steep peak of curves A and B1 did not occur again. The same experiment with the interruption (B1) was repeated and the sample was visually inspected. A red sample centre was observed which was surrounded by black material. This experiment will be referred to as the "archaeology experiment".

It was suspected that a limited heat transport in combination with a large heat production by the oxidation of soot was at least partly responsible for the observed phenomena. Therefore, sample sizes were decreased and the sample was diluted. Silicon

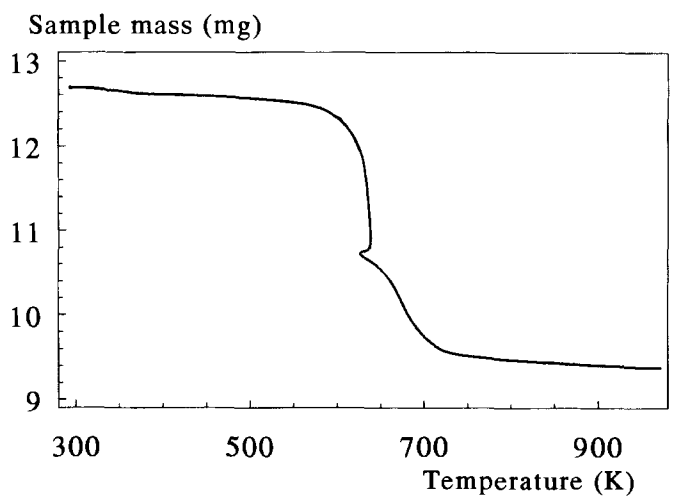

Fig. 2. Co_3O_4-catalysed combustion of Printex-U. a. As a function of temperature: —, sample mass. b. As a function of time. The temperature is shown on the right y-axis: – – –, DSC signal; —, temperature

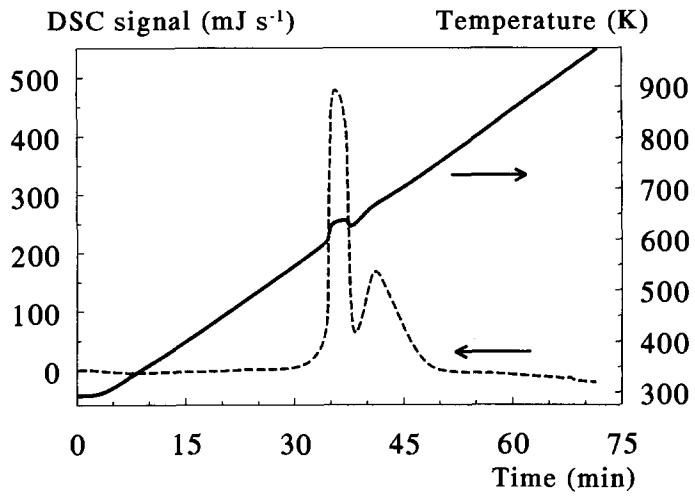

Fig. 2. (*Continued*)

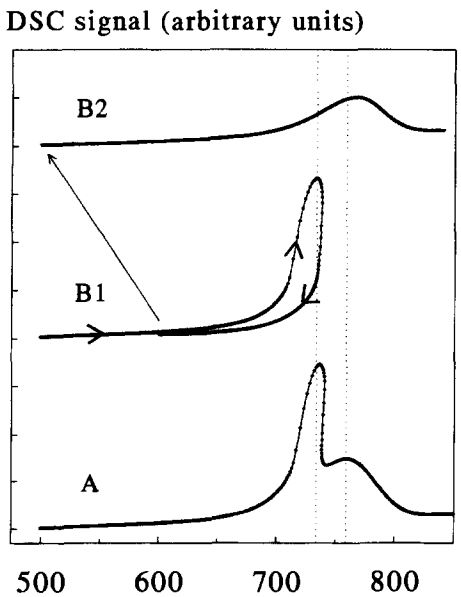

Fig. 3. Two combustion peaks with an Fe_2O_3 catalyst (A). A second experiment was stopped after the first peak (B1) and restarted after cooling down (B2).

carbide (SiC) was found to be suitable inert material with a high heat capacity and a high thermal conductivity. Smooth combustion peaks without large temperature effects in the sample during soot oxidation were measured when employing sample sizes of 2 mg soot and 4 mg catalyst, diluted with about 54 mg SiC. This is illustrated in Fig. 4 for an Fe_2O_3 catalyst.

The mass of an Fe_2O_3/Printex-U sample was found to have a large influence on the TGA/DSC curves, as is illustrated in Fig. 5. The DTG curves are scaled by division by the sample mass. The use of small samples of under 2 mg results in smooth combustion curves. For larger samples, part of the sample is combusted in a steep runaway peak, while the second part combusts at higher temperatures in a rather more normal peak. The temperatures at the maxima of these second peaks coincide reasonably well with the temperatures at the maxima of the peaks obtained for the smaller samples without the runaway peak. For even larger samples, the temperature at which the sample ignites further decreases, and the peak becomes broader. In these peaks, reaction rates exceed 1 mg min^{-1} for a short period of time and are about 1 mg min^{-1} in the rest of the peak. In the same figure, the DSC curves are plotted as dashed curves. The scaling is adapted; in all experiments the DSC curves have been divided by a constant facator of 33.33 J mg^{-1} in order to allow them to coincide with the DTG curves. This factor is close to the heat of combustion of graphite to CO_2 (32.765 J mg^{-1} [11]). At low sample masses, the scaled DSC curves coincide very well with the DTG curves. At increasing sample masses, DTG signals become larger than the scaled DSC curves at the beginning of the peaks. Apparently, the sample mass decreases not only as a result of soot oxidation, but also due to another reaction with a lower heat release. Near the end of the peaks, DTG and DSC curves again coincide.

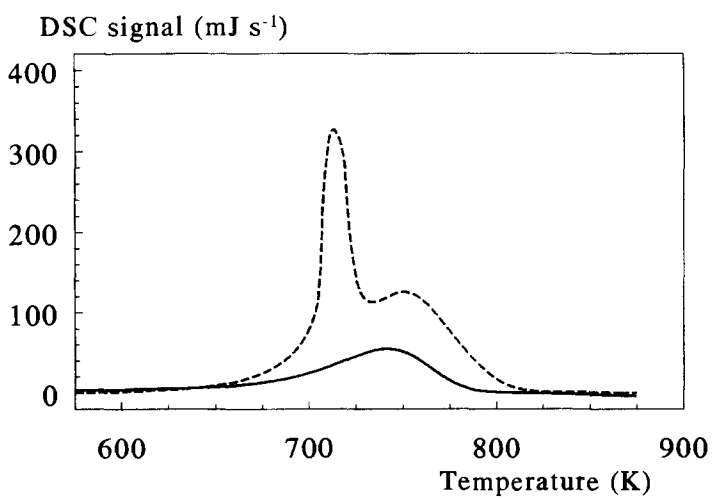

Fig. 4. Influence of sample size and dilution on TGA/DSC combustion pattern: ——, 2/4/54 mg; – – – 3.5/7/0 mg. Printex-U/Fe_2O_3/SiC, respectively.

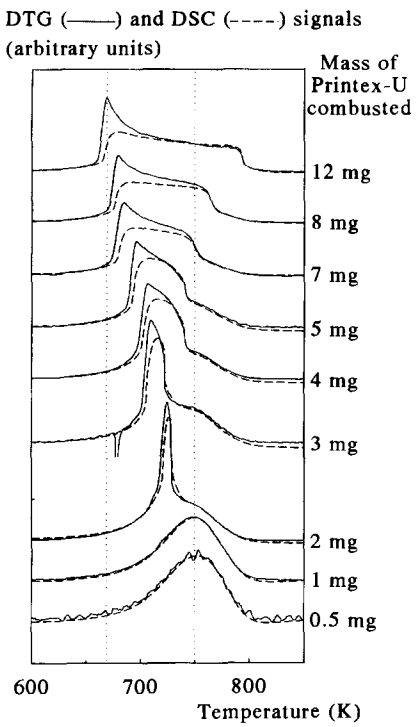

Fig. 5. Influence of sample mass on DTG (—) and DSC (– – –) curves for Fe_2O_3/Printex-U (tight contact). DSC curves are scaled to the DTG curves.

4.2. Simulations

The main parameters which determine the shape of the TGA/DTG curves in the numerical simulations were found to be the initial mass of Printex-U (M_C^0) and the sample heat conductivity (λ_{sample}). Results of simulations using combinations of M_C^0 of 1, 3.5, and 10 mg, with λ_{sample} values of 0.155, 0.309, 0.618, and 1.237 are shown in Fig. 6. A number of observations can be made from this figure. In the first place, the occurrence of a double-peaked combustion profile at lower heat conductivities is obvious. The double-peak form is more pronounced than the experimental results as shown in Fig. 5; the profiles resemble more closely the results obtained with Co_3O_4 catalysts as shown in Fig. 2. A second observation is that the profiles at a high Printex-U mass of 10 mg are very broad, and have maximum mass loss rates of 1 mg min^{-1}, which indicates that the soot oxidation is fully oxygen-mass-transfer-controlled. Indeed, the calculated relative oxygen concentration $[O_2]_{sample}/[O_2]_{bulk}$ during the simulation of these peaks is close to zero. A further observation is that for $M_C^0 = 1$ mg, the maximum of the second combustion peak always occurs around 750 K. At $M_C^0 = 3.5$ mg, this maximum is shifted to slightly higher temperatures at high values

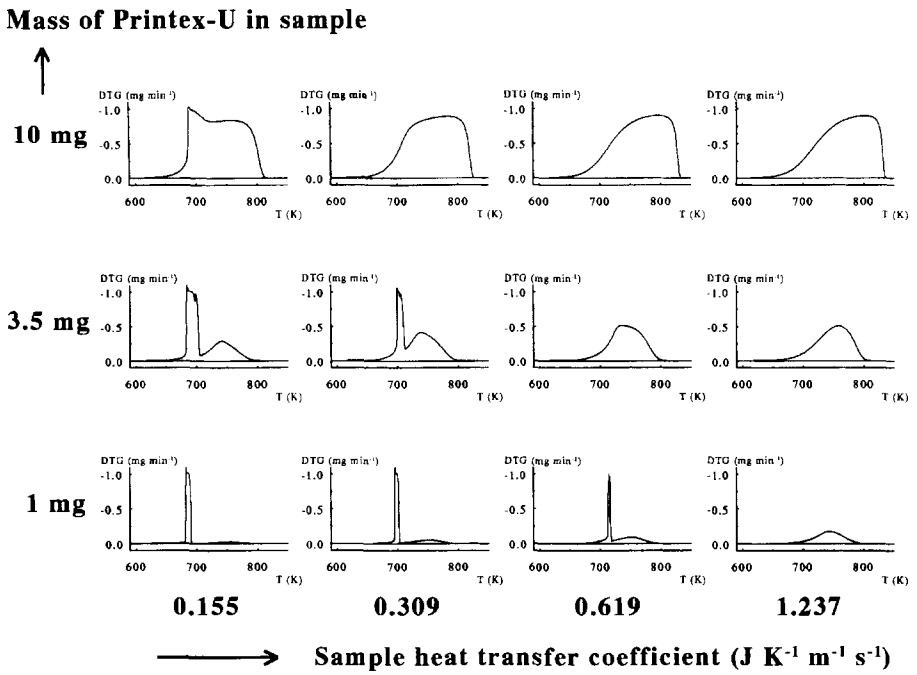

Fig. 6. Results of numerical simulation. DTG curves as a function of soot mass (= 1/3 sample mass) and sample heat conductivity.

for λ_{sample} and to lower values at low values for λ_{sample}. A last observation is the irregular form ("noise") of the DTG profile at the end of the high runaway peak at λ_{sample} values of 0.155 and 0.309 W m^{-1} K^{-1} for the 1 and 3.5 mg Printex-U samples, respectively.

In order to have a closer look at the simulated heat- and mass-transfer phenomena, the results of one of the calculations shown in Fig. 6, for $M_C^o = 3.5$ mg and $\lambda_{sample} = 0.309$ J m^{-1} K^{-1} s^{-1}, were studied in closer detail. Temperatures in the sample and the conversions of Printex-U are plotted in Figs. 7 and 8, respectively. Upper curves are simulation results for the innermost shell (the centre of the sample); the lower curves are results for shells at more outward positions in the sample. Results for the segments 1 (centre), 4, 7, 9, 11, 14, 17 and 20 (outer shell) are shown. The inset in Fig. 7 shows a detail of the temperatures in segments 5 to 12; the inset in Fig. 8 shows a detail of conversions in segments 1 to 7.

From Figs. 7 and 8, it is obvious that the two-peak combustion profiles are reflected in the temperature and conversion plots. In the first runaway peak, temperatures become very high and conversions in the inner shells rise very fast. At more outward positions in the sample, temperatures are much lower and conversions barely increase in the runaway peak. To understand the reason for the temperature drop in the sample at about 710 K, which demarcates the end of the runaway peak, oxygen concentrations and heat fluxes were considered. The total heat production is very large compared with

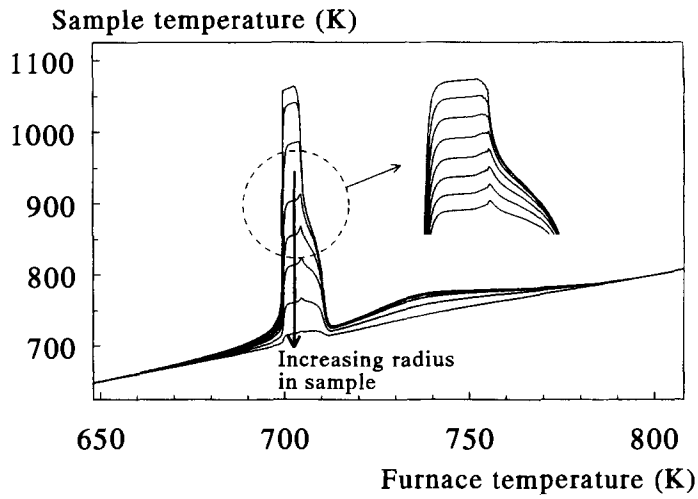

Fig. 7. Local sample temperatures as a function of TGA furnace temperature. Simulation with $\lambda_{sample} = 0.309\ J\ m^{-1}\ K^{-1}\ s^{-1}$ and $M_C^0 = 3.5$ mg. Segments 1, 4, 7, 9, 11, 14, 17 and 20 of 20 total. The inset shows segments 5 to 12.

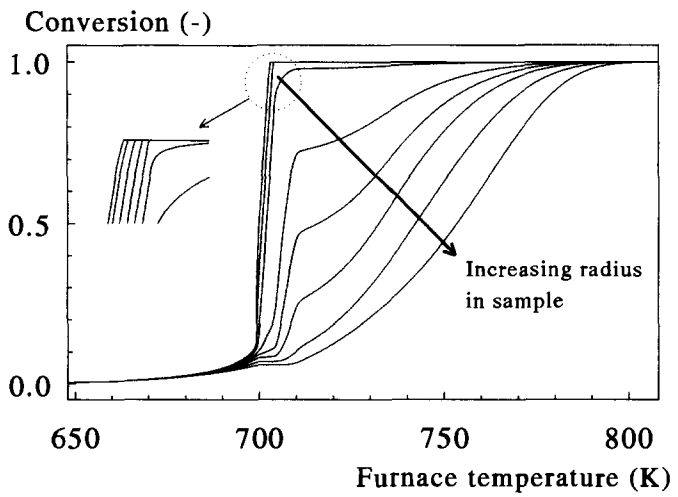

Fig. 8. Conversion of soot as a function of TGA furnace temperature. Simulation with $\lambda_{sample} = 0.309\ J\ m^{-1}\ K^{-1}\ s^{-1}$ and $M_C^0 = 3.5$ mg. Segments 1, 4, 7, 9, 11, 14, 17 and 20 of 20 total. The inset shows segments 1 to 7.

the heat needed to warm up the sample (the adiabatic temperature rise was calculated to be 9400 K!). As a results, a plot of heat fluxes does not give much information because the dominating heat flux is the heat transport from sample to gas bulk during the two combustion peaks. Fig. 9 shows the difference in the heat flux from and to the sample. This flux, which will be further denoted to as $\dot{Q}$, was calculated as the difference between the heat production by reactions (3), (4), (5), and the heat loss from the sample to the cup at the interface between sample and cup material, both in J s^{-1}. A positive value denotes a larger heat production than heat loss to the gas bulk, so that the sample temperature on average increases, whereas a negative value denotes a cooling down of the sample, as heat loss is larger than heat production. In the same figure, on the right-hand axis, the relative oxygen concentration is plotted. From Fig. 9 it can be observed that differences in heat production and heat loss are very pronounced in the region of the thermal runaway peak (698–712 K). A large sharp positive peak of $\dot{Q}$ is found at about 700 K (which is indicated by '2' in Fig. 9), which coincides with the temperature at which sample temperatures (Fig. 7) and conversions (Fig. 8) increase very steeply. Cooling down of the sample occurs in two steps: at about 704 K ('4' in Fig. 9, which coincides with the temperature at which Fe_3O_4, formed in the runaway reaction, is re-oxidized) and at about 710 K ('5' in Fig. 9). The oxygen concentration drops to very low values in the runaway peak. In the second combustion peak, $\dot{Q}$ is relatively small (over the total peak the signal is below 0.01 mJ s^{-1}). The relative oxygen concentration directly correlates with the reaction rate: $[O_2] \sim$ (constant-reaction rate).

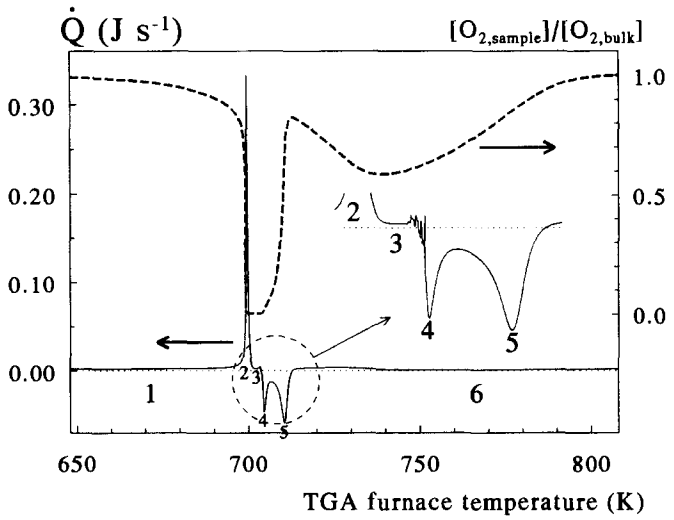

Fig. 9. Heat flux $\dot{Q}$ into sample (equals the difference between heat production into and loss from the sample) (—); and relative oxygen concentration (– – –). Simulation with $\lambda_{sample} = 0.309$ J m^{-1} K^{-1} s^{-1} and $M_C^0 = 3.5$ mg.

The influence of the order in oxygen concentration was assessed by varying this order in a number of simulations. Although an influence was found on the form of the second combustion peak, overall results were quite similar for orders in O_2 concentration of 1, 0.667, 0.5 and 0.25.

5. Discussion

5.1. Comparison of experimental and numerical results

One of the most striking observations is that the double-peaked TGA/DTG curves occur in both the experimental results and the numerical simulations. From the numerical results, it was concluded that a limited heat transport is at least partly responsible for these peculiar double-peak patterns, as the temperature which was measured under the sample cup significantly increased during the first combustion peak (Fig. 2b). Moreover, after the first combustion peak only the soot in the centre of the sample was found to be completely oxidized, whereas soot in the outer parts of the sample only reacted at higher temperatures (the "archaeology" experiment). It was anticipated that heat-transfer limitations alone cannot cause such peculiar combustion peaks, because one sharp combustion peak rather than a double-peak pattern would be expected if heat transfer is the only transport limitation. From the experimental results, it can also be seen that oxygen mass transfer plays a role, as the combustion profile gets broader at increasing sample sizes, and the DTG signal has a more or less constant value after an initial peak. Nor can oxygen mass-transfer limitations alone explain the experimental results, because under conditions of oxygen mass-transfer limitation the soot would combust in one, oxygen-mass-transfer-dominated combustion peak (as is the case for the higher sample masses in Fig. 5). The conclusion must be that in the double-peak patterns both heat- and mass-transfer limitations occur.

The numerical results are used to explain the reason for the double-peak patterns. In this explanation, the distinct periods within the two-peak combustion (indicated by the numbers in Fig. 9) are considered. In period (2) of Fig. 9, a thermal runaway occurs because the heat dissipation of the sample is slow compared with the heat that is generated by the reaction. The reaction rate then increases due to the higher temperatures, so that the reaction generates more heat, which again accelerates the reaction, etc. Temperatures in the centre of the sample then become very high (Fig. 7), and the reaction proceeds under oxygen mass-transfer-limited conditions in period (3) of Fig. 9 (the oxygen concentration is very small). As a larger temperature gradient exists in the sample, only the centre of the sample burns clean (Fig. 8). When the soot in the centre of the sample has burnt, soot oxidation proceeds in the more outer regions of the sample, and a gradual change in limitation of the reaction rate occurs: from oxygen mass-transfer limitation to a temperature-controlled reaction rate. This is explained in some detail. The region with complete or almost complete conversion in the centre of the sample will become larger when the conversion increases, and the contribution to total reaction rate of more outward situated segments will increase. As this 'reaction zone' shifts more and more to the outward-situated segments, the reaction rates decrease

because the temperature in the more outward-situated segments is lower compared with the centre. As a consequence, the oxygen concentration rises (as can be seen in Fig. 9). This then leads quickly to a cooling down of the sample by a sort of reversed thermal runaway: due to the lower reaction rates the heat production will decrease and therefore temperatures decrease; the reaction rates will then further decrease causing less heat production and a lower temperature, and so forth. This fast cooling down of the sample at 710 K (Fig. 7) causes the negative peak of the heat flux $\dot{Q}$ in period (5) in Fig. 9. Finally, in period (6) the soot in the outer regions is combusted in a quite normal combustion peak without high temperatures or large oxygen depletion. Observations as described in the "archaeology experiment" are explained in this way.

The "noise" at the end of period (3) in Fig. 9, the negative peak of $\dot{Q}$ in period (4) in Fig. 9, as well as the "noise" at the end of the runaway peaks in Fig. 6, are caused by re-oxidation Fe_3O_4 to Fe_2O_3. This re-oxidation occurs as soon as the conversion of soot in a segment is one (starting from the centre, segment 1, followed by segment 2, etc.). The limited amount of segments causes the "noise" at the end of period (4) in the insets of Figs. 7 and 9. A numerical simulation, in which reactions (4) and (5) were abandoned, resulted in quite similar results, the main difference being that this "noise" at the period (3) and the peak of period (4) in Fig. 9 did not occur.

5.2. *Parameter values*

The influence of sample mass is similar for experimental and numerical DTG curves. As the heat conductivity of the sample was not known exactly, model curves were calculated at different heat conductivities. The best qualitative comparison between experimental and model curves was obtained for high values of λ_{sample} for small samples, and for low values of λ_{sample} for larger samples. This can be explained from assumptions made in the derivation of the model. For small, very thin samples, the contribution of axial heat transport will be relatively large, as the surface in the radial direction (the "sides" of the cylindrical sample) is small compared with the bottom and top surface of the sample cylinder. For larger samples, the radial heat transport becomes more important at the cost of the axial heat transport contribution. Therefore, the actual λ_{sample} might be underestimated for small samples, and overestimated for large samples. As a result, the current model cannot draw quantitative conclusions concerning parameter values. Besides, it may be clear that the condition of a length-over-diameter ratio of 3 in the model description is not fulfilled.

5.3. *One-dimensional versus two-dimensional model description*

A more accurate description of heat and mass transport can be obtained if two-dimensional heat transport and oxygen mass transport are considered. As discussed above, heat dissipation would be facilitated by such a two-dimensional model and, therefore, runaways would occur only in calculations with lower heat conductivities. This influence would be largest for small samples and would decrease for larger samples. Considering the influence of the sample mass at a constant heat conductivity, results would coincide better with experimental DTG results.

It is, however, not considered useful to perform such detailed modelling. As many parameters influence the rates of heat and mass transfer, the outcome of such a detailed model would not be a general outcome, but would reflect the specific TA experiments for which parameter values were chosen. To assess the occurrence of heat- and mass-transfer limitations for another reaction in another TA apparatus, the modelling should be repeated with other parameter values. We do not believe this is meaningful, as the occurrence of heat- and mass-transfer limitations can be more easily assessed by experimental means, as will be explained in the next paragraphs. The model presented in this study should be used to understand observations that cannot be understood easily from experimental observations alone, e.g. the occurrence of the double-peak TGA/DSC pattern.

5.4. The need for small sample sizes in thermo-analytical techniques

It is concluded that for the model reaction of this study, the sample size is a very important parameter for the outcome of TGA/DSC experiments. The outcome of this study can be applied more generally in recommendations for TA techniques. Both heat- and mass-transport limitations can be important for all TA techniques, and practical guidelines can be given.

The occurrence of heat-transport limitations depends on physical parameters, the most important ones being the thermal conductivity of the cup material and its surroundings (the geometry of the TA apparatus), the thermal conductivity and heat capacity of the sample, and the heat of reaction of the sample together with the time scale of the reaction. If the temperature of the sample of the sample cup is measured, then heat-transport limitations can be very easily observed by a large temperature difference between oven temperature and the temperature of the sample or sample cup.

The occurrence of mass-transport limitations depends on the stoichiometry of the reaction (or adsorption/desorption), the time scale of these processes and the specific geometry of the sample, together with (to a lesser extent) the gas flow rate. It is impossible to observe directly the occurrence of mass-transfer limitations in a single TA experiment. It must be mentioned, however, that recently new TA techniques have been developed in which the sample is a packed bed, similar to a flow reactor (a pulse mass analyser, e.g. Refs. [15, 16]). Mass-transfer limitations (and to a lesser extent also heat-transfer limitations) will be reduced in such an apparatus compared with the more traditional TA techniques in which a sample cup is used.

The occurrence of both heat- and mass-transport limitations can be decreased by decreasing the sample size. Heat-transport limitations can also be decreased by dilution of the sample by a proper inert material such as silicon carbide. It is recommended that at the start of TA experiments, exploratory experiments are performed with varying sample masses, in order to define the window where heat- and mass-transfer limitations can occur. On the basis of the outcome of the present study, e.g. the results shown in Figs. 5 and 6, it is recommended that the sample size be varied by a factor of 10. Such a variation in sample mass will cause significant changes in the experimental results if heat-and/or mass-transfer limitations occur. Once it is verified that these limitations do not occur, the series of TA experiments should then be

performed with a sample size at the lower end of this range of sample masses. Of course, the sample material must be suitable for the use of small samples, e.g. materials with a large grain size are not.

Wilburn and Crighton [17] reported a numerical study from which they concluded that in suitably designed DTA apparatus the use of small samples is not that important. They did not, however, mention the value of the heat of reaction they used in their model, In our opinion, large samples can only be chosen if heats of reactions are relatively small and if depletion of reaction gases or accumulation of product gases does not easily occur. It is difficult to give general guidelines as many parameters play a role. Therefore, the above- mentioned initial series of experiments is recommended.

5.5. *Implications for other studies*

In the literature, a number of authors have obtained kinetic data from single-run TGA experiments, e.g. Ref. [18]. From the results of the present study, it can be concluded that this might given rise to erroneous results if heat- and mass-transfer limitations are not carefully considered and avoided.

The influence of the two transport limitations is even more difficult to interpret if the kinetics of the reaction under study are not known, and a function on the conversion χ, $f(\chi)$, in the equation $\delta\chi/\delta t = k_o \exp(-E_a/RT) f(\chi).\phi$ is chosen on the basis of conversion at DTG peak maximum and the width, onset temperature and final temperature of the DTG peak [19, 20]. The peak maximum conversion was found to be more or less constant at different heating rates ϕ, which forms the basis of a simple criterion for selection of this $f(\chi)$ which has been reported in the literature [20]. As has been described in more detail elsewhere (chapter 4 of Ref. [7]), heat- and mass-transport limitations might have a considerable effect on this peak maximum conversion, and do, therefore, also influence the validity of this selection method for the kinetic equation $f(\chi)$.

The present study shows the importance of heat- and mass-transfer limitations in TGA. The model which is used gives qualitative information on the relevance of these two transport limitations. It is difficult and also not useful to give general guidelines for the conditions under which such limitations might be expected, as the geometry and material of the TA apparatus are important. We feel, however, that recognition of these limitations is important and that quantitative data from TGA runs cannot be properly obtained without due consideration of these transport limitations.

6. Conclusions

A model was developed which describes heat and oxygen mass transfer in a TGA sample. This model was evaluated with a specific case study: the catalytic oxidation of soot. Experimental and numerical results were found to agree very well qualitatively.

It was shown by experimental data and by numerical simulations that the sample size is an important parameter in thermo-analytical experiments. It was argued that large samples can cause limitations of both heat- and mass-transfer, which can

drastically influence the results of these experiments. Therefore, small samples should be used when heat- and mass-transfer limitations occur at higher sample masses. The occurrence of these limitations depends on several parameters, which complicate general guidelines for sample size or sample dilution to avoid these limitations. Numerical simulations can be a tool for the determination of these limitations, but as it is difficult to determine some of the important parameters accurately, e.g. the heat conductivity of the sample, it is more practical to determine these limitations experimentally. Therefore, it is recommended that at the start of each series of TA experiments the occurrence of heat- and mass-transfer limitations is checked by variation of the sample size by at least a factor of ten.

An explanation was found for the often observed double-peak combustion profiles, first a sharp runaway peak and the second, a smooth combustion peak. These profiles are a result of combined heat- and mass-transport phenomena.

References

[1] F. Kapteijn, G.B. Marin and J.A. Moulijn, Catalytic reaction engineering, in J.A. Moulijn, P.W.N.M. van Leeuwen and R.A. van Santen (Eds.), Catalysis. An Integrated Approach to Homogeneous, Heterogeneous and Industrial Catalysis, Elsevier, Amsterdam, 1993, p. 251.
[2] T. Wigmans, H. van Cranenburgh, R. Elfring and J.A. Moulijn, Carbon, 21 (1983) 21.
[3] F. Bonnefoy, P. Gilot, B.R. Stanmore and G. Prado, Carbon, 32 (1994) 1333.
[4] B. Stanmore, P. Gilot and G. Prado, Thermochim. Acta, 240 (1994) 79.
[5] P.A. Morgan, S.D. Robertson and J.F. Unsworth, Fuel, 65 (1986) 1546.
[6] R. Melling, F.W. Wilburn and R.M. McIntosh, Anal. Chem., 41 (1969) 1275.
[7] J.P.A. Neeft, Catalytic oxidation of soot. Potential for the reduction of diesel particulate emissions, Ph.D. thesis, Delft University of Technology, Delft, 1995.
[8] G.V. Samsonov, The Oxide Handbook, IFI/Plenum, New York, 1973.
[9] A.M. James and M.P. Lord, Macmillan's Chemical and Physical Data, Macmillan Press, London, 1992.
[10] R.C. Weast and M.J. Astle, Handbook of Chemistry and Physics, 62nd edn., CRC Press, Inc., Boca Raton, Florida, 1981.
[11] R.H. Perry and D. Green, Perry's Chemical Engineers' Handbook, 10th edn., McGraw-Hill, New York, 1984.
[12] E.A. Heintz and W.E. Parker, Carbon, 4 (1966) 473.
[13] M.C. Abraham and A. Ghosh, Ironmaking and Steelmaking, (1979) 14.
[14] R.J. Fruehan, Metallurg. Trans. B, 8B (1977) 279.
[15] F. Hershkowitz and P.D. Madiara, Ind. Eng. Chem. Res., 32 (1993) 2969.
[16] S.C. Fung, C.A. Querini, K. Liu, D.S. Rumschitzki and T.C. Ho, In situ coking kinetics obtained from a new flow through microbalance and reaction kinetics monitored by GC, in B. Delmon and G.F. Froment (Eds), Catalyst Deactivation 1994, Elsevier Science BV, Amsterdam, 1994, p. 305.
[17] F.W. Wilburn and J.S. Crighton, Thermochim. Acta, 188 (1991) 315.
[18] J.C. Frohne, H. Reisig and H.-K. Schädlich, Erdöl Kohle, Erdgas, Petrochem., 42 (1989) 152.
[19] D. Dollimore, T.A. Evans, Y.F. Lee, G.P. Pee and F.W. Wilburn, Thermochim. Acta, 196 (1992) 255.
[20] D.Dollimore, T.A. Evans, Y.F. Lee and F.W. Wilburn, Thermochim. Acta, 198 (1992) 249.